



Kent Academic Repository

Moss, Rob M., Pickup, David M., Ahmed, Ifty, Knowles, Jonathan C., Smith, Mark E. and Newport, Robert J. (2008) *Structural characteristics of antibacterial bioresorbable phosphate glass*. *Advanced Functional Materials*, 18 (4). pp. 634-639. ISSN 1616-301X.

Downloaded from

<https://kar.kent.ac.uk/15920/> The University of Kent's Academic Repository KAR

The version of record is available from

<https://doi.org/10.1002/adfm.200700721>

This document version

UNSPECIFIED

DOI for this version

Licence for this version

UNSPECIFIED

Additional information

Versions of research works

Versions of Record

If this version is the version of record, it is the same as the published version available on the publisher's web site. Cite as the published version.

Author Accepted Manuscripts

If this document is identified as the Author Accepted Manuscript it is the version after peer review but before type setting, copy editing or publisher branding. Cite as Surname, Initial. (Year) 'Title of article'. To be published in *Title of Journal*, Volume and issue numbers [peer-reviewed accepted version]. Available at: DOI or URL (Accessed: date).

Enquiries

If you have questions about this document contact ResearchSupport@kent.ac.uk. Please include the URL of the record in KAR. If you believe that your, or a third party's rights have been compromised through this document please see our [Take Down policy](https://www.kent.ac.uk/guides/kar-the-kent-academic-repository#policies) (available from <https://www.kent.ac.uk/guides/kar-the-kent-academic-repository#policies>).

Structural Characteristics of Antibacterial Bioresorbable Phosphate Glass**

By Robert M. Moss,* David M. Pickup, Ifty Ahmed, Jonathan C. Knowles, Mark E. Smith, and Robert J. Newport

Neutron diffraction with isotopic substitution has been used to probe the local environment of silver in a melt-quench derived bioresorbable phosphate glass. Samples enriched with ^{107}Ag and ^{109}Ag were prepared and neutron diffraction data collected. A first-order difference was taken between the data sets to give detailed information about the silver environment in the glass matrix. The measured Ag-O correlation has three components in the first coordination shell at 2.28 Å, 2.51 Å, and 2.58 Å with coordination numbers of 2.1, 2.7, and 1.1, respectively, consistent with silver occupying a distorted octahedral environment. These results have been correlated with those from Ag K-edge X-ray absorption near-edge spectroscopy measurements. The results suggest that the addition of silver to the $(\text{CaO})_{0.3}(\text{Na}_2\text{O})_{0.2}(\text{P}_2\text{O}_5)_{0.5}$ system has a significant effect on the host phosphate network, with shorter and more branched chains replacing the long chains and rings normally associated with the metaphosphate composition.

1. Introduction

The incidence of biomaterial-centered infection, often leading to revision surgery, underlies the need to improve the properties of existing biomaterials. At present, prophylaxis, often in the form of systemically administered antibiotics, is the main weapon against bacterial infection following implant surgery. An approach to circumvent the problems associated with the use of antibiotics would be to incorporate antimicrobial agents into device materials. In particular, there is a need to use antimicrobial agents that are effective against biofilms-complex aggregations of microorganisms marked by the excretion of a protective and adhesive matrix, which have been found to be involved in a wide variety of microbial infections in the body.^[1] Silver exerts a biocidal effect against a wide range of microbes including *Staphylococcus aureus*, *Escherichia coli*, *Pseudomonas aeruginosa*, *Candida albicans* and methicillin-resistant *Staphylococcus aureus* (MRSA).^[2]

For this reason silver has been investigated *in vitro* and *in vivo* for use in wound dressings^[3] and catheters.^[4] Furthermore, silver-doped hydrated sodium aluminosilicates have been investigated for dental applications because of their antibacterial properties.^[5] Alumina substrates have also been coated with silver-based materials by both ion beam assisted deposition^[6] and electrochemical deposition^[7] in order to impart antibacterial qualities.

Phosphate-based glasses containing ions routinely found in the human body (such as Ca^{2+} and Na^+) can be classed as bioresorbable and biocompatible. In the ternary P_2O_5 -CaO- Na_2O system, it has been shown that the dissolution rate varies reciprocally with the CaO concentration.^[8] Furthermore, ternary phosphate glasses with a high CaO content (>24 mol %) show excellent *in vitro* biocompatibility^[9] with a significant increase in cell proliferation relative to the control, and being entirely amorphous there is little risk of residual fragments causing sterile inflammation. There is much interest in fibers manufactured from these glasses for potential use in tissue engineering applications, and in particular those involving tissue with a medium to high anisotropy, such as muscle and ligament.^[10] Tubes have also been produced which have been used in the repair of severed nerves in facial tissue.^[11]

Bioresorbable phosphate-based glasses incorporating silver ions are potential materials for antibacterial devices. The wide spectrum of solubility offers potential applications as temporary devices where a second device removal operation would therefore not be necessary. This property also offers a mechanism by which the antibacterial metal ions are released in a controlled way from the network. Degradation studies of these glasses have shown that the silver ions are released slowly and continuously over time when in contact with an aqueous medium.^[12] Initial cell work has shown that the antibacterial effectiveness of these glasses does not vary smoothly with silver concentration. Figure 1 shows that glasses containing ≥ 15 mol % Ag_2O are less effective than those with lower silver content;

[*] R. M. Moss, Dr. D. M. Pickup, Prof. R. J. Newport
School of Physical Sciences, University of Kent
Canterbury, Kent, CT2 7NH (UK)
E-mail: rmm25@kent.ac.uk

Dr. I. Ahmed, Prof. J. C. Knowles
Division of Biomaterials and Tissue Engineering
UCL Eastman Dental Institute
London, WC1X 8LD (UK)

Prof. M. E. Smith
Department of Physics, University of Warwick
Coventry, CV4 7AL (UK)

[**] The authors wish to thank the EPSRC (EP/P502543, EP/C000714, EP/C00633/1, GR/T21080/01) and STFC (CMPC06103) for funding, and the use of the EPSRC Chemical Database Service at the STFC Daresbury Laboratory. We are grateful for the insight and help provided by Prof. A. C. Hannon of ISIS, STFC Rutherford Appleton Laboratory.

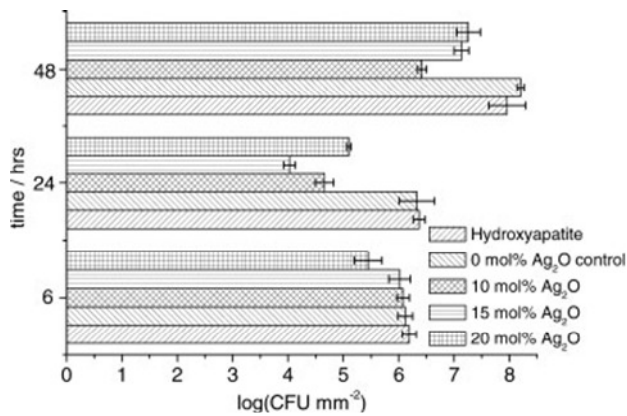


Figure 1. The variation of number of culture forming units (CFU) per unit area for *Staphylococcus aureus* in biofilms, given as a function of time and silver content. Data from [12].

the same study also showed that the chemical durability of the glass increased with silver content, resulting in a reduced rate of silver ion release.^[12] This latter result was used to explain the diminished antimicrobial properties at higher silver content: it was concluded that the increase in chemical durability was a result of a structural change related to the silver content.

To better understand and to optimize the antibacterial action of silver-doped phosphate based glasses it is necessary to study the structure of the glass network and to focus in particular on the local environment of the silver sites. Previous work on such samples has shown that this information cannot reliably be obtained by other methods. Standard diffraction methods using both neutrons (ND) and X-rays (XRD) do not reveal information about Ag–O bonding due to overlap of the real-space correlations in the region 2.2 to 2.6 Å. Ag K-edge extended X-ray absorption fine structure spectroscopy, EXAFS, and X-ray absorption near edge spectroscopy, XANES, also suffer limitations in this regard. The XANES measurements can reveal variations in coordination numbers and/or local symmetry around the silver site between samples, but cannot yield definitive structural parameters.^[13] The EXAFS results are inconclusive due to the weak Ag K-edge EXAFS oscillations, which are a consequence of silver ions occupying very disordered sites in this type of material.^[14] Neutron diffraction with isotopic substitution (NDIS) utilizes

the variation in scattering length between isotopes of the same element: thus, by using two samples with identical compositions and structures, but differing silver isotopes, it is possible to isolate the silver contributions to the network.^[15]

2. Results and Discussion

Measurements of the glass composition and density show that the two samples of $(\text{CaO})_{0.3}(\text{Na}_2\text{O})_{0.1}(\text{Ag}_2\text{O})_{0.1}(\text{P}_2\text{O}_5)_{0.5}$ are identical in these basic respects (within the experimental error) except for the silver isotope used in the preparation. The results of this analysis are shown in Table 1. Their structural equivalence was demonstrated using high energy X-ray diffraction.

To obtain structural information from the raw neutron diffraction data it was necessary to remove the background scattering and perform corrections for absorption and multiple scattering to find the differential cross-section.

$$\frac{d\sigma}{d\Omega} = i(Q) + I_s(Q) \quad (1)$$

where $Q = 4\pi\sin\theta/\lambda$ (2θ is the scattering angle and λ is the neutron wavelength). After removal of the calculated self-scattering term, $I_s(Q)$, the resultant coherent scattering intensity or interference function, $i(Q)$ was Fourier transformed to yield the total correlation function, $T(r)$.

$$T(r) = T^0(r) + \frac{2}{\pi} \int_0^\infty Qi(Q)M(Q)\sin(Qr)dQ \quad (2)$$

$M(Q)$ is the window function that takes into account the finite experimentally obtainable value of Q . $T^0(r)$ is the average density term, given by:

$$T^0(r) = 4\pi r \rho^0 \left(\sum_i c_i b_i \right)^2 \quad (3)$$

where r represents the scalar distance between pairs of atoms, ρ^0 is the macroscopic number density and c_i and b_i are the concentration and coherent scattering length of the i^{th} atom respectively. The pair distribution function that results from a neutron diffraction experiment, $T(r)$, can be represented as the weighted sum of partial correlation

Table 1. Sample characterization of melt-quench prepared $^{107/109}\text{Ag}$ doped phosphate glasses.

Sample	Measured composition [atm%] (± 0.1)					Density [gcm^{-3}] (± 0.05)
	P	O	Ca	Na	Ag	
^{107}Ag doped glass	21.6	64.1	5.9	4.5	3.9	2.88
^{109}Ag doped glass	21.5	64.0	5.8	4.7	3.9	2.81

functions, $t_{ij}(r)$.

$$T(r) = \sum_{ij} c_i c_j b_i b_j t_{ij}(r) \quad (4)$$

Examining Equation 4, it can be seen that, if samples are prepared that are identical except for the scattering length of one element, differences between the neutron scattering data from these samples will isolate the partial correlation functions. Since different isotopes of an element have different scattering lengths, isotopic substitution provides a method for achieving this separation.

In the work presented here, the scattering length of silver was varied between a pair of otherwise identical samples by isotopic substitution. The difference in real space can be represented in terms of the partial pair correlation function, $t'_{Aj}(r)$, such that only the environment of element A is probed.

$$\begin{aligned} T_{A-j}(r) &= T(r) - T'(r) \\ &= c_A^2 (b_A^2 - b_A'^2) t'_{AA}(r) + 2 \sum_{j \neq A} c_A c_j b_j (b_A - b_A') t'_{Aj}(r) \end{aligned} \quad (5)$$

Structural information can be obtained by modeling the real-space correlation function. Pair functions, $p_{ij}(Q)$, are generated in Q -space and Fourier transformed to allow comparison with the experimental data in real space. The pair functions are given by:

$$p_{ij}(Q) = \frac{N_{ij} w_{ij} \sin(QR_{ij})}{c_j Q R_{ij}} \exp\left[\frac{-Q^2 \sigma_{ij}^2}{2}\right] \quad (6)$$

where N_{ij} , R_{ij} , and σ_{ij} are the coordination number, atomic separation and disorder parameter (i.e., a measure of static and thermal disorder) respectively of atom i in relation to atom j . The weighting factors w_{ij} for a standard neutron diffraction experiment are given by:

$$w_{i \neq j} = 2c_i c_j b_i b_j \quad (7)$$

$$w_{i=j} = c_i^2 b_i^2 \quad (8)$$

In the case of the isotopic difference the weighting factors take different forms:

$$w_{A \neq j} = 2c_A c_j (b_A - b_A') b_j \quad (9)$$

$$w_{A=j} = c_A^2 (b_A^2 - b_A'^2) \quad (10)$$

In this case atom A is silver. Silver has two naturally occurring stable isotopes which have roughly equal abundances: ^{107}Ag has a neutron scattering length of $b_A = 7.555$ fm and ^{109}Ag has $b'_A = 4.165$ fm.

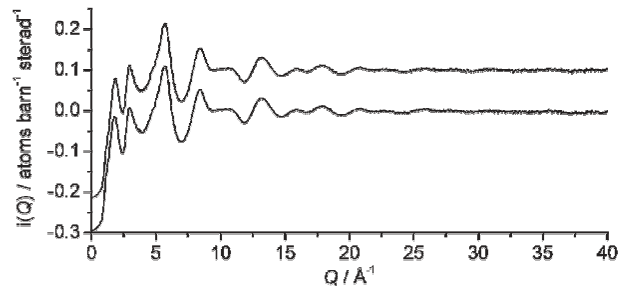


Figure 2. Neutron diffraction Q -space interference functions, $i(Q)$, measured for the ^{107}Ag (upper) and ^{109}Ag (lower) doped phosphate glasses. The ^{107}Ag $i(Q)$ is off-set by $+0.1$ atoms $\text{barn}^{-1} \text{sterad}^{-1}$ for clarity.

The ND interference functions, $i(Q)$, from the two $(\text{CaO})_{0.3}(\text{Na}_2\text{O})_{0.1}(\text{Ag}_2\text{O})_{0.1}(\text{P}_2\text{O}_5)_{0.5}$ glass samples are shown in Figure 2. It was necessary to limit Q_{max} of the individual datasets to 40 \AA^{-1} because of the significant effect at high Q of the large absorption cross-sections of both silver isotopes. Fourier transformation of the $i(Q)$ curves gave the real-space correlation functions, $T_{107}(r)$ and $T_{109}(r)$. Figure 3 shows the difference correlation function, $T_{\text{Ag-j}}(r)$, obtained by taking the first-order difference, $T_{107}(r) - T_{109}(r)$. The structural parameters obtained by fitting the difference correlation function using the method described previously are shown in Table 2. Figure 4 shows the total correlation functions for the two samples after having the Ag- j correlations removed. Table 3 contains the structural parameters obtained by fitting these functions. As expected from two structurally equivalent samples, these parameters are identical within experimental error.

The distances and coordination numbers obtained from the $T_{\text{Ag-j}}(r)$ function are consistent with the silver ions occupying a site surrounded by a distorted octahedron of oxygen atoms. There are three discrete Ag-O distances in the first coordination shell at 2.28 \AA , 2.51 \AA , and 2.58 \AA with associated coordination numbers of 2.1, 2.7, and 1.1, respectively. This suggests that the silver ions occupy highly disordered sites within the glass matrix. Similar disordered sites are found in

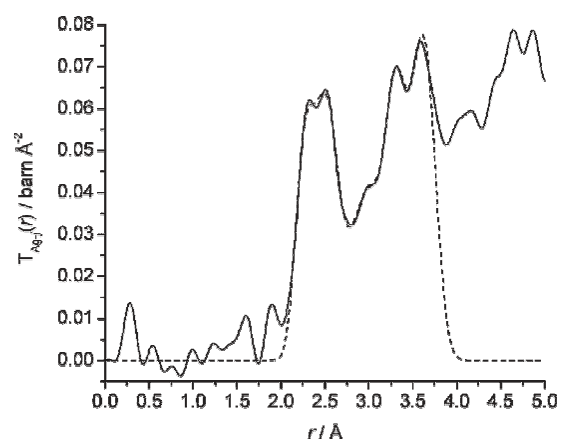


Figure 3. Difference pair correlation function, $T_{\text{Ag-j}}(r)$, for the experimentally measured (solid) and the simulated (dashed) functions.

Table 2. Ag-*j* correlations determined by fitting the difference $T_{Ag-j}(r)$. Correlations shown with ... separators represent nearest neighbors which are not directly bonded; i.e., the Ag...O correlation is considered to be in the second coordination sphere. The values of R, N, and σ correspond to the respective parameters in Equation 6.

Correlation	R [Å] (± 0.03)	N (± 0.5)	σ [Å] (± 0.03)
Ag-O	2.28	2.1	0.08
Ag-O	2.51	2.7	0.09
Ag-O	2.73	1.1	0.10
Ag...O	2.99	2.5	0.12
Ag...P	3.31	6.0	0.11

crystalline materials containing polyphosphate chains (e.g., $AgBa(PO_3)_3$, Ag_2HPO_4 and $AgZn(PO_3)_3$).^[16–18] To put these NDIS results in a wider context, we collected XANES and EXAFS data from a series of glasses prepared by the same method, but with varying silver content, i.e., $(CaO)_{0.3} \cdot (Na_2O)_{0.2-x} \cdot (Ag_2O)_x \cdot (P_2O_5)_{0.5}$, where $x = 0.05, 0.10, 0.15$ and 0.20 . The observed degree of disorder is qualitatively supported by the Ag K-edge EXAFS data, which only exhibited very weak EXAFS oscillations, despite cooling the samples to ca. 77 K. Ag K-edge XANES measurements on the same samples proved more informative.^[12,19] The data shown in Figure 5 reveals that there is no variation in the shape or position of the absorption edge as a function of silver content. The position of the Ag K-edge in our samples is identical to that of the reference material Ag_2SO_4 , indicating identical oxidation states; the shape of the spectra are also similar. Thus, on the basis of the spectra shown in Figure 5, it may be concluded that these glasses contain Ag^I ions in a structural environment very similar to that of silver in Ag_2SO_4 and that there is no change in this environment as a function of silver content. Since silver in Ag_2SO_4 resides in a distorted octahedral site with two short Ag–O bond-lengths of 2.39 Å, two intermediate Ag–O bond-lengths of 2.44 Å and two long

Table 3. Structural parameters obtained by fitting the $T(r)$ functions. The Ag-*j* correlations were fixed with the values shown in Table 2. Correlations shown with ... separators represent nearest neighbors which are not directly bonded. The values of R, N, and σ correspond to the respective parameters in Equation 6.

Sample	Correlation	R [Å] (± 0.01)	N (± 0.2)	σ [Å] (± 0.01)
¹⁰⁷ Ag doped glass	P-NBO	1.48	1.9	0.06
	P-BO	1.60	1.9	0.06
	Na-O	2.33	3.4	0.13
	Ca-O	2.38	4.0	0.10
	O...O	2.51	4.0	0.10
	O...O	2.81	0.7	0.11
¹⁰⁹ Ag doped glass	P...P	2.93	2.2	0.08
	P-NBO	1.48	1.9	0.06
	P-BO	1.60	1.9	0.06
	Na-O	2.33	3.5	0.13
	Ca-O	2.38	4.1	0.11
	O...O	2.51	4.1	0.10
	O...O	2.82	0.6	0.11
	P...P	2.93	2.2	0.08

Ag–O bond-lengths of 2.66 Å,^[14] it may now be surmised that silver occupies a qualitatively similar site in the isotopically substituted glasses. Hence, the results of the NDIS experiment are in agreement with those from the XANES study – and in addition provide data of significantly enhanced quantitative reliability across a broader set of length scales, and relating to all atom-pairs present in the glass.

Furthermore, the $T_{Ag-j}(r)$ function also reveals information about the second Ag...O coordination sphere and the first Ag...P nearest-neighbor distance. The distances obtained from the fitting process of 2.99 Å and 3.21 Å, respectively, are consistent with those observed in crystalline polyphosphate materials containing Ag^I ions of similar composition.^[17]

The parameters in Table 3 for the P–O, Na–O, Ca–O, O–O, and P–P correlations are typical of those from a metapho-

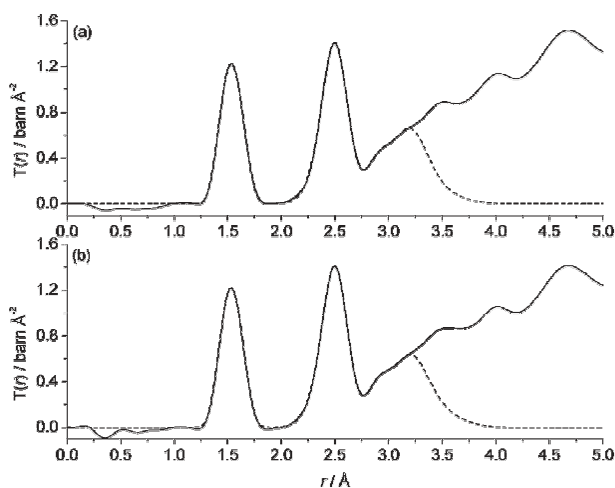


Figure 4. Total correlation functions, $T(r)$, with the Ag-*j* correlations removed (solid) for a) ¹⁰⁷Ag and b) ¹⁰⁹Ag doped samples. The real space simulation (dashed) is shown for each sample.

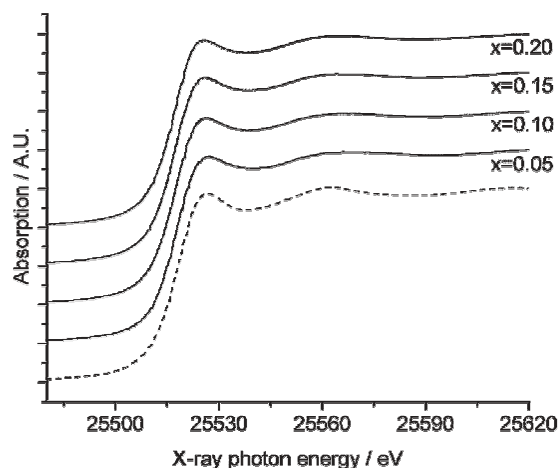


Figure 5. Ag K-edge XANES for samples of composition $(CaO)_{0.3} \cdot (Na_2O)_{0.2-x} \cdot (Ag_2O)_x \cdot (P_2O_5)_{0.5}$. The spectrum for Ag_2SO_4 is also shown (dashed) for comparison. Spectra for $x = 0.05$ and 0.10 are reproduced from ref. [19] and ref. [12], respectively.

Table 4. P–NBO and P–BO bond length variation for different Qⁿ speciation and cations modifiers in crystalline and amorphous samples. Parameters taken from [a] ref. [15], [b] ref. [16], and [c] ref. [18].

Q ⁿ species	Compound	Form	Bond length [Å]	
			P–NBO	P–BO
Q ¹	Na ₄ P ₂ O ₇	Crystalline	1.51 ^a	1.63 ^a
	Ca ₂ P ₂ O ₇	Crystalline	1.52 ^a	1.62 ^a
Q ²	NaPO ₃	Crystalline	1.48 ^a	1.61 ^a
	NaPO ₃	Amorphous	1.48 ^b	1.61 ^b
	CaP ₂ O ₆	Crystalline	1.49 ^a	1.58 ^a
	CaP ₂ O ₆	Amorphous	1.49 ^b	1.60 ^b
	Ca ₂ NaP ₅ O ₁₅	Amorphous	1.49 ^b	1.60 ^b
Q ³	v-P ₂ O ₅	Amorphous	1.43 ^c	1.58 ^c

osphate glass.^[20] Phosphate glasses have network structures comprised of interconnected PO₄³⁻ tetrahedra. The PO₄³⁻ connectivity is best described by the Qⁿ notation where *n* is the number of bridging oxygen atoms (BOs) per tetrahedral unit. Vitreous P₂O₅ (v-P₂O₅) is composed entirely of Q³ connected tetrahedra such that each unit is connected to three more via BOs. The addition of oxides, such as CaO, act as network modifiers with the metal ions disrupting the P–O–P bonding, resulting in the presence of non-bridging oxygen atoms (NBOs) and the formation of Q¹ and Q² groups.^[8,21,22] In metaphosphate glasses, i.e., those having compositions with O/P = 3, the phosphate tetrahedra are arranged in Q² rings and chains with ionic cross-linking holding these moieties together. The primary peak at about 1.55 Å in the *T(r)* functions shown in Figure 4 is due to P–O bonding within the PO₄³⁻ tetrahedra. Two distinct P–O distances are observed in phosphate-based glasses: a shorter distance of ca. 1.49 Å ascribed to bonds with NBOs and a longer distance of ca. 1.60 Å due to bonds with BOs.

Comparing the disorder parameters for these bonds ($\sigma_{\text{P-NBO}}$ and $\sigma_{\text{P-BO}}$, derived from the width of the relevant pair correlation peak) given in Table 3, which both have values of 0.06 Å, with those measured in a previous study of (CaO)_{0.5-x}(Na₂O)_x(P₂O₅)_{0.5} glasses,^[20] of $\sigma_{\text{P-NBO}} = 0.03$ Å and $\sigma_{\text{P-BO}} = 0.05$ Å, we see there is significantly more disorder in the P–NBO bonding in the silver-doped glasses. The origin of this difference is related to the connectivity of the PO₄³⁻ tetrahedra. In a previous ³¹P solid state NMR study of (CaO)_{0.3}(Na₂O)_{0.2-x}(Ag₂O)_x(P₂O₅)_{0.5} glasses it was observed that the relative concentration of Q¹ and Q³ species increases with silver content.^[12] This result suggested that the addition of Ag^I ions to the matrix causes disproportionation of the phosphate groups according to 2Q² → Q¹ + Q³. It was suggested that this structural change was responsible for an increase in the chemical durability of the glass and reduced dissolution rate of the silver ions, which resulted in decreased antimicrobial potency.^[12] Note that Q¹ units represent P₂O₇⁴⁻ dimers and chain-terminating phosphate groups, whereas Q³ units are representative of cross-links between phosphate chains. The increase in the $\sigma_{\text{P-BO}}$ with the

addition of silver observed here provides clear evidence that disproportionation is occurring. This can be understood by considering the nature of the P–NBO bonds in the various Qⁿ species using a simple bond order model.^[23] Given that the phosphorus valence can be considered as +5 and the oxygen valence as –2, the P–NBO bond order ($\eta_{\text{P-NBO}}$) can be calculated from the simple expression $\eta_{\text{P-NBO}} = (5 - N_{\text{BO}}) / N_{\text{NBO}}$, where *N*_{BO} and *N*_{NBO} are the number of bridging and non-bridging oxygens per unit. For Q¹, Q², and Q³ units $\eta_{\text{P-NBO}}$ is 1.33, 1.5, and 2.0 respectively. It is expected that the P–NBO distance will vary inversely with the bond order. Table 4 lists the P–NBO bond distances for the Qⁿ species found in crystalline and amorphous sodium and calcium phosphates and confirms the variation of P–NBO distance with bond order. Hence, if disproportionation occurs in phosphate-based glasses the increase in the number of Qⁿ species present will introduce static disorder into the P–NBO bonding, as observed here.

The O...O distances measured give information on the PO₄, CaO_x, and NaO_x polyhedra that comprise the structure. Taking an average P–O bond length of 1.54 Å and assuming a tetrahedral angle of 109°, the calculated average O...O distance for the PO₄ group is 2.51 Å which agrees exactly with the shorter O...O distance measured here. The longer O...O distance is probably associated with the separation between phosphate groups which are not directly connected to each other, but this assignment remains tentative. The structural parameters for the Ca–O and Na–O correlations are consistent with those previously found in similar phosphate-based glasses.^[20,21]

3. Conclusions

Neutron diffraction with isotopic substitution has been used to reveal three distinct Ag–O distances in (CaO)_{0.3}–(Na₂O)_{0.1}(Ag₂O)_{0.1}(P₂O₅)_{0.5} melt-quench derived glass. The results are consistent with silver being in a highly distorted octahedral environment and agree with those from Ag K-edge XANES measurements on (CaO)_{0.3}(Na₂O)_{0.2-x}(Ag₂O)_x(P₂O₅)_{0.5} glasses, where *x* = 0.05, 0.10, 0.15, and 0.20. Since the XANES spectra exhibited no variation as a function of silver content, we can conclude that the silver ions, Ag^I, adopt this environment at all the compositions studied. The introduction of silver ions causes disproportionation of phosphate network-forming units. The Q² rings and chains that are normal for metaphosphate glasses are transformed into Q¹ and Q³ units. This is confirmed by the broadening of the P–NBO correlation compared to glasses containing no silver. It is this subtle change in the network structure, not observed directly hitherto, that is likely to be the cause of the decreased biocidal efficacy of the glass at higher silver contents.

4. Experimental

Sample Preparation for NDIS: The glass samples were prepared using NaH₂PO₄, CaCO₃, P₂O₅ (BDH, UK) and isotopically

enriched Ag_2SO_4 as starting materials. Two samples of Ag_2SO_4 were prepared from 98.9 at % enriched ^{107}Ag and 99.4 at % enriched ^{109}Ag metal (STB Isotope, Germany) using the following method. First the powdered metal (1 g) was dispersed in deionized water (4.6 ml) before adding concentrated nitric acid (2.75 ml, BDH, UK) drop wise, whilst stirring. After 15 min., when the silver metal had dissolved and the solution cooled, a stoichiometric amount of 5 M H_2SO_4 standard solution (0.92 ml, Sigma–Aldrich, UK) was added using a pipette. After a further 1 h, the precipitation of Ag_2SO_4 was complete. The H_2O and HNO_3 were removed from the precipitate at 40 °C using a vacuum line and a water bath to supply the heat. The resultant powder was dried under vacuum for 1.5 hrs at 300 °C using a heating mantle. As a final drying step, the Ag_2SO_4 powder was placed in an oven at 250 °C overnight.

Two 6 mm diameter $(\text{CaO})_{0.3}(\text{Na}_2\text{O})_{0.1}(\text{Ag}_2\text{O})_{0.1}(\text{P}_2\text{O}_5)_{0.5}$ glass rods were prepared using the isotopically enriched Ag_2SO_4 . The precursors were weighed out into a 30 ml silica crucible (Saint-Gobain, U.K.), mixed and the crucible loaded into a preheated furnace. The mixture was left at 300 °C for half an hour, raised to 600 °C for a further half hour and finally melted at 1200 °C for one hour. The molten glass was then poured into a 6 mm diameter graphite mould, which had been preheated to 370 °C. The mould was then left to cool slowly to room temperature in order to remove any residual stress.

Similar materials produced by the melt-quenching method have been shown to contain silver nano-particles. [24] Absorption bands are seen in the UV-vis spectra at 200–230 nm and 400–500 nm in the presence of even small concentrations of metallic nano-particles, which refer to silver electronic transitions and surface plasmon resonances, respectively. [25] The UV-spectra from the samples prepared here were measured on a Cary 400 Scan UV-Visible Spectrophotometer and no evidence of silver nano-particulates was observed.

Neutron Diffraction with Isotopic Substitution: The data presented here were collected on the GEM diffractometer at the ISIS pulsed neutron source at the Rutherford Appleton Laboratory, UK. The solid glass rods were mounted on a sample holder and placed directly in the beam. Time-of-flight data was collected over a large Q -range (up to 50 \AA^{-1}). The program *Gudrun* was used to perform the data reduction and corrections. [26]

Since the results of a NDIS experiment depend on taking a difference between data from different samples it was essential that the samples prepared were identical in composition and structure except for the isotope of silver present. The sample composition was measured by a commercial company (Medac Ltd) using ICP-AES and the macroscopic density was measured by helium pycnometry using a Quantachrome Multipycnometer. The results of this analysis are given in Table 1. In order to check the structural equivalence of the two samples, high energy X-ray diffraction (HEXRD) data were collected on Station 9.1 at the Synchrotron Radiation Source (SRS), Daresbury Laboratory, UK. The results confirmed that the two samples were structurally identical within the errors associated with the HEXRD measurements.

Ag K-Edge XANES/EXAFS: Measurements were made on Station 16.5 at the Synchrotron Radiation Source (SRS) Daresbury Laboratory, UK, with synchrotron ring energy of 2 GeV and a stored current of 150–250 mA. The spectra were recorded in transmission mode using a double crystal Si(220) monochromator ($d = 1.92 \text{ \AA}$). The incident beam intensity, i_0 , and the transmitted beam intensity, i_t , were measured using ionization chambers. The transmission spectrum for a silver foil was measured using a third ionization chamber. The energy scale was defined by assigning the maximum of the derivative of the silver foil spectrum to 25521.0 eV. Finely-ground samples were diluted in polyethylene (Aldrich, spectrophotometric grade) and pressed into pellets to give a satisfactory K-edge absorption step. The pellets were mounted in a liquid N_2 cryostat cooled to $\sim 77 \text{ K}$. The sample end of the

cryostat was placed in a vacuum chamber while the XANES/EXAFS spectra were collected over a sufficiently large range to allow accurate background subtraction. The data processing comprised conversion of i_0 and i_t to absorption, calibration of the energy scale and removal of the background. The continuum absorption was removed by fitting a straight line to the pre-edge and a low-order polynomial to the post-edge regions. The absorption step for all spectra was normalized to unity.

Received: July 4, 2007

Revised: November 13, 2007

- [1] P. S. Stewart, J. W. Costerton, *Lancet* **2001**, 358, 135.
- [2] I. Ahmed, D. Ready, M. Wilson, J. C. Knowles, *J. Biomed. Mater. Res. Part A* **2006**, 79, 618.
- [3] K. H. Hong, *Polym. Eng. Sci.* **2007**, 47, 43.
- [4] T. Gilchrist, D. M. Healy, C. Drake, *Biomaterials* **1991**, 12, 76.
- [5] K. Kawahara, K. Tsuruda, M. Morishita, M. Uchida, *Dent. Mater.* **2000**, 16, 452.
- [6] Q. Ling Feng, T. Nam Kim, J. Wu, E. Seo Park, J. Ock Kim, D. Young Lim, F. Zhai Cui, *Thin Solid Films* **1998**, 335, 214.
- [7] G. J. Chi, S. W. Yao, J. Fan, W. G. Zhang, H. Z. Wang, *Surf. Coat. Technol.* **2002**, 157, 162.
- [8] J. C. Knowles, *J. Mater. Chem.* **2003**, 13, 2395.
- [9] V. Salih, K. Franks, M. James, G. W. Hastings, J. C. Knowles, I. Olsen, *J. Mater. Sci. Mater. Med.* **2000**, 11, 615.
- [10] I. Ahmed, C. A. Collins, M. P. Lewis, I. Olsen, J. C. Knowles, *Biomaterials* **2004**, 25, 3223.
- [11] T. Gilchrist, M. A. Glasby, D. M. Healy, G. Kelly, D. V. Lenihan, K. L. McDowall, I. A. Miller, L. M. Myles, *Br. J. Plast. Surg.* **1998**, 51, 231.
- [12] S. P. Valappil, D. M. Pickup, D. L. Carroll, C. K. Hope, J. Pratten, R. J. Newport, M. E. Smith, M. Wilson, J. C. Knowles, *Antimicrob. Agents Chemother.* **2007**, 51, 4453.
- [13] O. Siper, G. Dalba, F. Rocca, *Phys. Rev. B* **2004**, 69, 134201.
- [14] D. A. Fletcher, R. F. McMeeking, D. Parkin, *J. Chem. Inf. Comput. Sci.* **1996**, 36, 746.
- [15] J. C. Wasse, I. Petri, P. S. Salmon, *J. Phys. Condens. Matter* **2001**, 13, 6165.
- [16] I. Belharouak, H. Aouad, M. Mesnaoui, M. Maazaz, C. Parent, B. Tanguy, P. Gravereau, G. Le Flem, *J. Solid State Chem.* **1999**, 145, 97.
- [17] M. T. Averbuchpouchot, A. Durif, *J. Solid State Chem.* **1983**, 49, 341.
- [18] I. Tordjman, A. Boudjada, J. C. Guitel, R. Masse, *Acta Crystallogr.* **1978**, 34, 3723.
- [19] I. Ahmed, E. A. Abou Neel, S. P. Valappil, S. N. Nazhat, D. M. Pickup, D. Carta, D. L. Carroll, R. J. Newport, M. E. Smith, J. C. Knowles, *J. Mater. Sci.* **2007**, 42, 9827.
- [20] D. M. Pickup, I. Ahmed, P. Guerry, J. C. Knowles, M. E. Smith, R. J. Newport, *J. Phys. Condens. Matter* **2007**, 19, 415116.
- [21] R. K. Brow, *J. Non-Cryst. Solids* **2000**, 263, 1.
- [22] U. Hoppe, *J. Non-Cryst. Solids* **1996**, 195, 138.
- [23] U. Hoppe, G. Walter, R. Kranold, D. Stachel, *J. Non-Cryst. Solids* **2000**, 263, 29.
- [24] L. Baia, M. Baia, W. Kiefer, J. Popp, S. Simon, *Chem. Phys.* **2006**, 327, 63.
- [25] L. Baia, D. Muresan, M. Baia, J. Popp, S. Simon, *Vib. Spectrosc.* **2007**, 43, 313.
- [26] A. C. Hannon, *Nucl. Instrum. Methods Phys. Res. Sect. A* **2005**, 551, 88.